Electronic Supplementary Information

Nuclear localization of dirhodium(II) complexes in breast cancer cells by X-ray fluorescence microscopy

Alejandra Enriquez Garcia[†], Barry Lai[‡], Sesha Gopal Gopinathan[§], Hugh H. Harris[‖], Carrie S. Shemanko[§], and Farideh Jalilehvand*[†]

[†] Department of Chemistry, University of Calgary, Calgary, AB T2N 1N4, Canada.

[‡] Advanced Photon Source, X-ray Science Division, Argonne National Laboratory, Argonne, IL 60439, USA.

[§] Department of Biological Sciences, University of Calgary, Calgary, AB T2N 1N4, Canada.

[‖] Department of Chemistry, The University of Adelaide, SA 5005, Australia.

Table of Contents

Experimental Section S3-6

Scheme S1. Schematic of an X-ray fluorescence microscopy setup, similar to the one employed in this study. S6

Figure S1. ^{1}H NMR spectrum of a solution of $[Rh_2(AcO)_2(Met)_2]\cdot 5H_2O$ (**2**) in D_2O S7

Figure S2. ^{13}C NMR spectrum of a solution of $[Rh_2(AcO)_2(Met)_2]\cdot 5H_2O$ (**2**) in D_2O S7

Figure S3. ^{1}H NMR spectrum of a solution of $[Rh_2(OAc)_2(bpy)_2](AcO)_2$ (**3**) in D_2O S8

Figure S4. ^{13}C NMR spectrum of a solution of $[Rh_2(OAc)_2(bpy)_2](AcO)_2$ (**3**) in D_2O S8

Figure S5. *Left*) (+)-Ion mode ESI-mass spectra of $[Rh_2(AcO)_2(Met)_2]\cdot 5H2O$ (**2**) and *right*) assignment of the corresponding mass peaks S9

Figure S6. *Left*) (+)-Ion mode ESI-mass spectra of $[Rh_2(OAc)_2(bpy)_2](AcO)_2$ (**3**) and *right*) assignment of the corresponding mass peaks S9

Figure S7. Cell viability plots for MDA-MB-231 cells treated with $Rh_2(AcO)_4$ (**1**), $[Rh_2(AcO)_2(Met)_2]\cdot 5H_2O$ (**2**) and $[Rh_2(AcO)_2(bpy)_2](AcO)_2$ (**3**). S10

Figure S8. Dose-response curves for MDA-MB-231 cells treated with $Rh_2(AcO)_4$ (**1**), $[Rh_2(AcO)_2(Met)_2]\cdot 5H_2O$ (**2**) and $[Rh_2(AcO)_2(bpy)_2](AcO)_2$ (**3**). S11

Figure S9. Optical micrographs and XFM maps for MDA-MB-231 control cells S12

Figure S10. Optical micrographs & XFM maps for MDA-MB-231 treated with **1** (6 hrs) S13

Figure S11. Optical micrographs and XFM maps for MDA-MB-231 treated with **2** (6 hrs) S14

Figure S12. Optical micrographs and XFM maps for MDA-MB-231 treated with **3** (6 hrs) S15

Figure S13. Intracellular content of P, S, Cl, K, Ca, Fe, Cu, Zn, and Rh for MDA-MB-231 S16 cells treated with $Rh_2(AcO)_4$ (**1**), $[Rh_2(AcO)_2(Met)_2]\cdot 5H_2O$ (**2**), and $[Rh_2(AcO)_2(bpy)_2](AcO)_2$ (**3**) for 6 hrs compared to control cells.

Table S1. Quantified average intracellular and nuclear Rh content for MDA-MB-231 S17 cells treated with $Rh_2(AcO)_4$ (**1**), $[Rh_2(AcO)_2(Met)_2]\cdot 5H_2O$ (**2**) and $[Rh_2(AcO)_2(bpy)_2](AcO)_2$ (**3**)

Table S2. Dipole moments obtained from the DFT calculations performed on the S17 optimized geometries of $Rh_2(AcO)_4$ (**1**), $[Rh_2(AcO)_2(Met)_2]$ (**2**) and $[Rh_2(AcO)_2(bpy)_2]^{2+}$.

Figure S14. XFM spectra compared with the fittings for sample cells treated for 6 hrs with S18 $Rh_2(AcO)_4$ (**1**), $[Rh_2(AcO)_2(Met)_2]\cdot 5H_2O$ (**2**), $[Rh_2(AcO)_2(bpy)_2](AcO)_2$ (**3**), and control cells

Figure S15. Optical micrographs & XFM maps for MDA-MB-231 treated with **1** (1 hr) S19

References S20

Experimental Section

Sample Preparation. Dirhodium(II) tetraacetate (pure; 47% Rh, **1**) was obtained from Pressure Chemical Company and used as supplied. $[Rh_2(OAc)_2(Met)_2]\cdot 5H_2O$ (**2**) was synthesized as previously reported by our group[1] and $[Rh_2(OAc)_2(bpy)_2](AcO)_2$ (**3**), following a reported literature procedure.[2]

*Synthesis of $[Rh_2(OAc)_2(Met)_2]\cdot 5H_2O$ (**2**).* Solid DL-methionine (0.452 mmol) was added to an aqueous solution of $Rh_2(AcO)_4$ (0.226 mmol). The resulting violet solution was stirred at 100°C for 24 h, then concentrated to 2 mL, and passed through a Sephadex G-15 size exclusion chromatography column using distilled water as eluent. The purple band was isolated and evaporated to dryness resulting in a purple solid. Yield: 35%. Elemental anal. calcd for $[Rh_2(AcO)_2(Met)_2]\cdot 5H_2O$ ($Rh_2C_{14}H_{36}N_2O_{13}S_2$): %C 23.67, %H 5.11, %N 3.94 (12.7% H_2O); Found %C 23.61, %H 4.97, %N 3.94 (TG: 13.1% H_2O). ^{1}H NMR (400 MHz, D_2O): δ_H (ppm) = 3.74 (t, 2H), 3.06 (dt, 2H), 2.81 (td, 2H), 2.52 (dq, 2H), 2.29 (s, 3H), 2.10−2.20 (m, 2H), 2.14 (s, 6H), 2.11 (s, 3H). ^{13}C NMR (400 MHz, D_2O): δ_C (ppm) = 19.4 (SCH_3), 22.4 $(CH_3COO)_{ave}$, 27.8, 32.6 (SCH_2CH_2), 58.4 ($CHNH_2$), 181.4 (Met-COO), 189.7 $(CH_3COO)_{ave}$.

*Synthesis of $[Rh_2(OAc)_2(bpy)_2](AcO)_2$ (**3**).* Solid 2,2'-bipyridine (0.452 mmol) was added to a violet solution of $Rh_2(AcO)_4$ (0.226 mmol) in acetonitrile. The resulting mixture was refluxed at 100°C for 24h. The resulting red solid was isolated by vacuum filtration. Yield: 57%. Elemental anal. calcd for $[Rh_2(OAc)_2(bpy)_2](AcO)_2$ ($C_{28}H_{28}N_4O_8Rh_2$) : C, 44.58; H, 3.74; N, 7.42. Found: C, 44.20; H, 3.75; N, 7.47. ^{1}H NMR (400 MHz, D_2O): δ_H (ppm) = 1.96 (s, 3H), 2.61 (s, 3H), 7.44 (td, 2H), 7.92-8.00 (m, 4H), 8.35 (d, 2H). ^{13}C NMR (400 MHz, D_2O): δ_C (ppm) = 23.6 (CH_3COO), 123.6, 128.0, 139.9, 151.7, 156.5 (bpy), 191.8 (CH_3COO).

NMR Spectroscopy. All ^{1}H and ^{13}C NMR measurements were performed using a Bruker Avance III 400 MHz spectrometer. ^{13}C NMR spectra were collected using a 30° pulse, a 26.2 kHz sweep width, a 1-s delay between scans, and 65 K data points. A total of 1000 scans were coadded for better signal-to-noise ratio. In the case of the spectrum of 2 performed in D_2O, the peaks were externally calibrated using CH_3OH in D_2O, resonating at 49.15 ppm.[3] ^{1}H NMR spectra were collected by coadding 64 scans and internally referenced using the HOD/H_2O peak at 4.80 ppm.[4]

ESI-Mass Spectrometry. Electrospray ionization (ESI) mass spectra were collected both in positive (+) and negative (−) ion modes on an Agilent 6520 Q-Tof instrument. All samples were dissolved in water and diluted in MeOH before injection and mobilization using an injection flow

rate of 0.2 mL/min and a drying gas flow rate of 7 L/min at 200 °C. Capillary, skimmer, and fragmentor voltages were set at 4000, 65, and 80 V, respectively.

Cell culture. MDA-MB-231 breast cancer cells were from the ATCC and aliquots cultured for not longer than 6 months after thawing. Cells were cultured in Dulbecco's Modified Eagle Medium (DMEM) supplemented with 10% v/v fetal bovine serum (FBS), Streptomycin (100 μg/mL), Penicillin (100 Units/mL) and L-glutamine (2 mM). Cells were maintained in culture plates of 10 cm diameter at 37°C and 5% CO_2, and subcultured every 3-4 days.

Cell viability assay. Cell viability was assessed using the resazurin-based Alamar blue assay. Briefly, cells were seeded (7,500 cells/well) in a black-walled 96-well plate and were allowed to attach for at least 36 hr at 37 ^{0}C with 5% CO_2 before treatment. Media was then replaced by either fresh new media (for the control) or media containing different concentrations of the drugs **1-3** and left for 48 hr at 37 ^{0}C with 5% CO_2. After treatment, cells were washed with PBS and treated with a solution of 10% v/v Alamar blue reagent in media for 2.5 hr at 37 ^{0}C in a 5% CO_2-humidified incubator. Fluorescence from the resorufin salt formed was read using a Spectramax M4 Microplate Reader using an excitation wavelength between 550-570 nm and an emission wavelength between 590-600 nm. Cell viability was reported as percentage of the fluorescence of a specific sample with respect to the control. IC_{50} values were calculated using GraphPad Prism Version 5.03 software[5] by curve-fitting plots of cell viability (%) vs. log of drug concentration.

X-ray fluorescence microscopy sample preparation. Samples for XFM were prepared by plating MDA-MB-231 cells on 1.5 mm x 1.5 mm x 500 nm silicon nitride windows (Silson Ltd., UK) in 6-well plates (3mL, 75,000 cells/mL). Cells were allowed to adhere over a period of 36 hr at 37 ^{0}C in a 5% CO_2-humidified incubator. Solutions of **1-3** in DMEM were prepared (200 μM) fresh before treatment. Such concentration was chosen to obtain reasonable signal from the drug inside the cells. Lower concentrations closer to the IC_{50} of **1** (40 μM) were tested, but no Rh fluorescence signal could be detected. Cells were then treated with these solutions as well as just DMEM as control for a 6 hr period. At the end of the treatment, cells were washed with PBS and then fixed with a 4% paraformaldehyde solution (prepared in fresh D-PBS) for 1 hour in an incubator at 37 °C and 5% CO_2. The windows containing the fixed cells were then washed twice with a solution of ammonium acetate in Milli-Q water (100 mM) and air dried covered overnight. The samples were stored in a desiccator until transported to the beamline.

The 6 hr treatment time was chosen to maximize drug accumulation and minimize drug efflux from the cells. In cancer cells, this process is mediated by the so-called ABC transporters, many of which are involved in the release of chemotherapeutic drugs (thereby reducing drug accumulation) and the acquisition of multidrug resistance.[6, 7] Several studies have reported a correlation between ABC transporter expression and invasive chemo-resistant cancers.[8, 9] For MDA-MB-231 cancer cells, the over- expression of some ABC transporters (as compared to 60 other cancer cell lines) provides reason to believe that these cells may employ this mechanism to eliminate xenobiotic compounds such as the dirhodium(II) complexes, therefore limiting the time these drugs remain in the cell.[10, 11]

Spectroscopic data collection. XFM imaging of the cells was performed at the Advanced Photon Source beamline 2-ID-D (Argonne National Laboratory, Lemont, IL). The X-ray energy was tuned to 23.8 keV using a double multilayers monochromator to excite the Kα emission lines of Rh. To increase the focusing efficiency at such high energy, two Fresnel zone plates were aligned in near field, which focused the X-ray beam to a spot size of ca. 0.35 μm on the sample. An additional X-ray energy tuning to 12.8 KeV was necessary to detect the Kα emission lines with high sensitivity for elements up to Zn. The same Fresnel zone plate was used to focus the X-ray beam at the lower energy. An energy-dispersive silicon drift detector (Vortex EM, SII Nanotechnology, Northridge, California, USA) was used to collect the X-ray fluorescence spectra from the sample, which was place in a He environment at 75° to the incident beam. All elemental maps were recorded using the step-scan mode, with a 0.5 μm step-size, a 1000 ms dwell time for the Rh map and 300 ms dwell time for all other elements.

X-ray fluorescence microscopy data analysis. Elemental maps as well regions of interest (ROIs) were generated with the MAPS software package[12] by Gaussian fitting of the raw emission spectra for each image pixel. The Gaussian peaks were matched to characteristic X-ray emission lines to determine the fluorescence signal for each element. Quantification of the data (in $\mu g/cm^2$) was performed by comparing the X-ray fluorescence intensity to those from NBS thin film standards 1832, NBS-1833 (National Institute of Standards and Technology, Gaithersburg, MD, USA). Rhodium quantification was performed by comparing the fluorescence from the sample with that of a Rh standard (1.25 $\mu g/cm^2$ from Micromatter Technologies Inc., Surrey, BC, Canada).

Computational calculations. The Gaussian 16 (G16) package was used to optimize all molecular structures and determine their dipole moment.[13] Initial atomic coordinates were imported from the

crystal structures of $[Rh_2(AcO)_4(H_2O)_2]$,[14] $[Rh_2(OAc)_2(Met)_2]$[1] and $[Rh_2(OAc)_2(bpy)_2(CH_3CN)_2](PF_6)_2 \cdot 2CH_3CN$.[2] For the former, the axial aqua ligands were removed and for the latter, the PF_6 counterions as well as the coordinated and non-coordinated acetonitrile ligands were removed prior to calculation. The vibrational frequencies were calculated to confirm that the optimized structures corresponded to minima on the potential energy surface. All density functional theory (DFT) optimizations were performed using the BHANDHLYP functional, the 6-31G(d) basis set for non-metal atoms and the LANL2DZ pseudopotential for the rhodium ions.

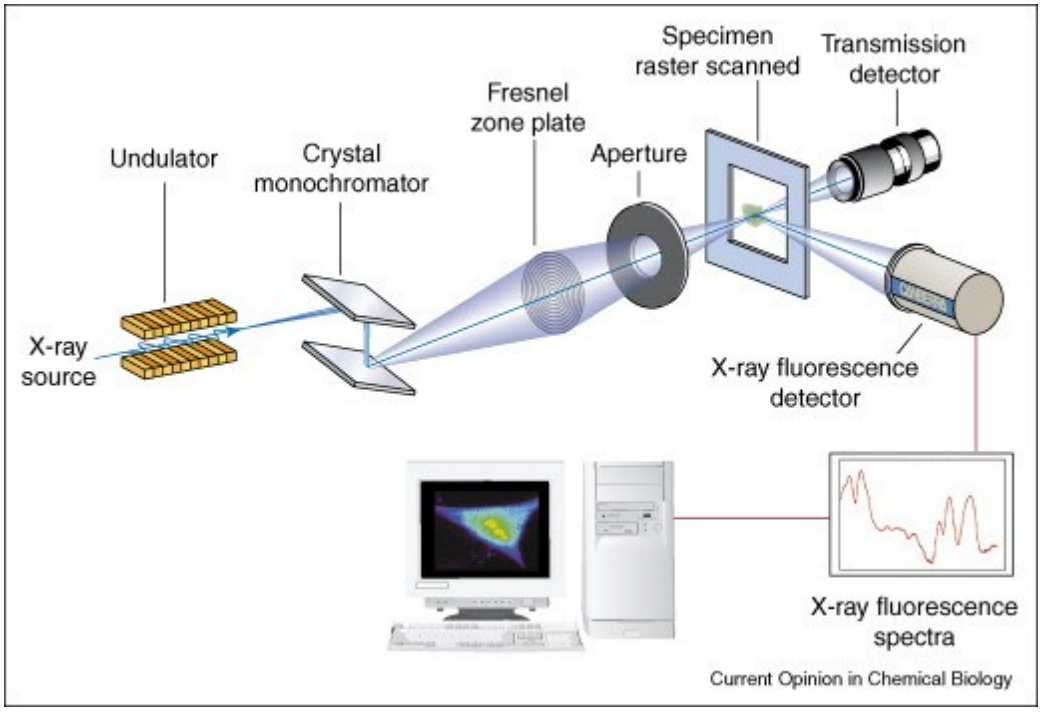

Scheme S1. Schematic of an X-ray fluorescence microscopy setup, similar to the one employed in this study (Reproduced with permission from Reference 15).

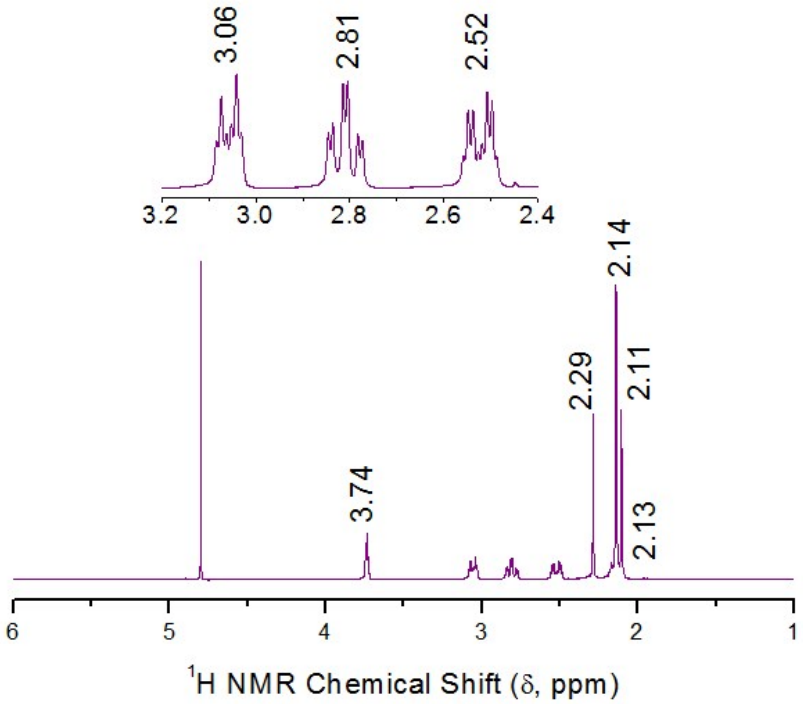

Figure S1. ^{1}H NMR spectrum of a solution of $[Rh_2(AcO)_2(Met)_2]\cdot 5H_2O$ (**2**) in D_2O.

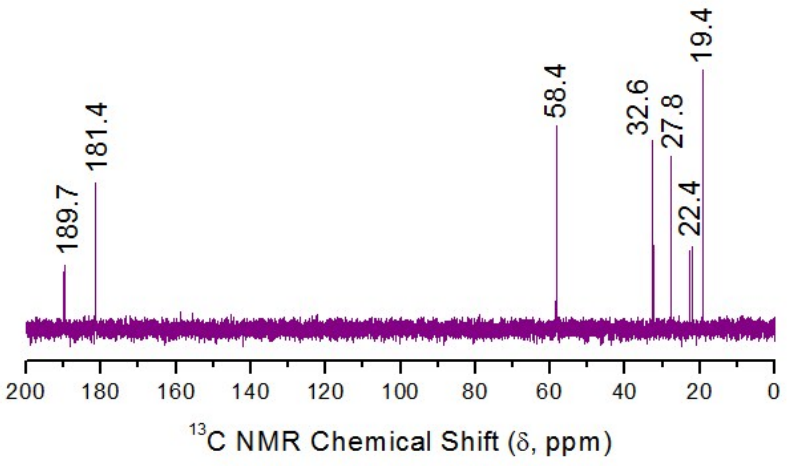

Figure S2. ^{13}C NMR spectrum of a solution of $[Rh_2(AcO)_2(Met)_2]\cdot 5H_2O$ (**2**) in D_2O.

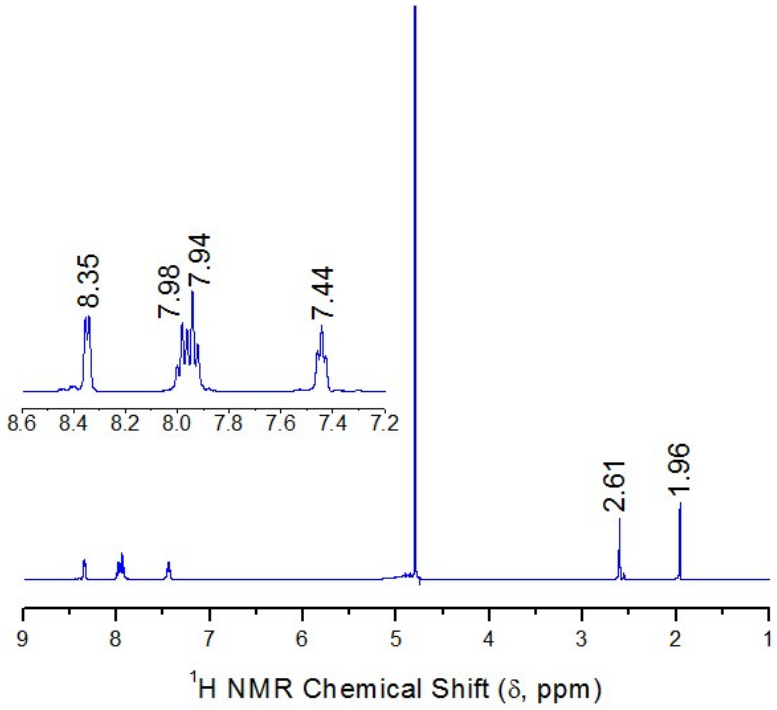

Figure S3. ^{1}H NMR spectrum of a solution of $[Rh_2(OAc)_2(bpy)_2](AcO)_2$ (**3**) in D_2O.

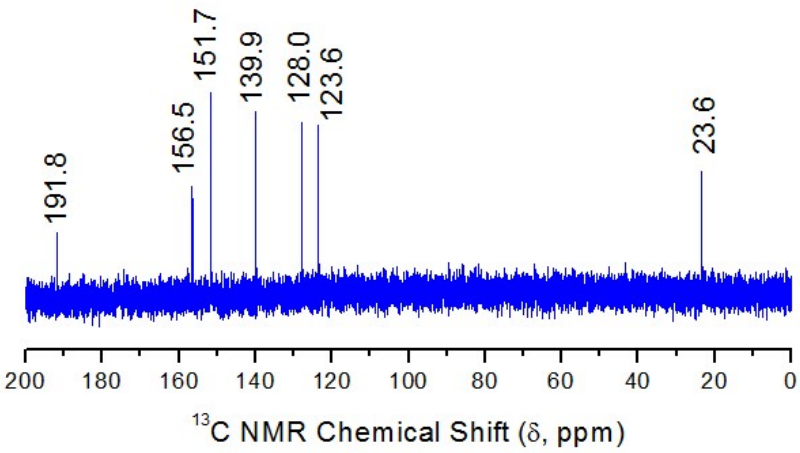

Figure S4. ^{13}C NMR spectrum of a solution of $[Rh_2(OAc)_2(bpy)_2](AcO)_2$ (**3**) in D_2O.

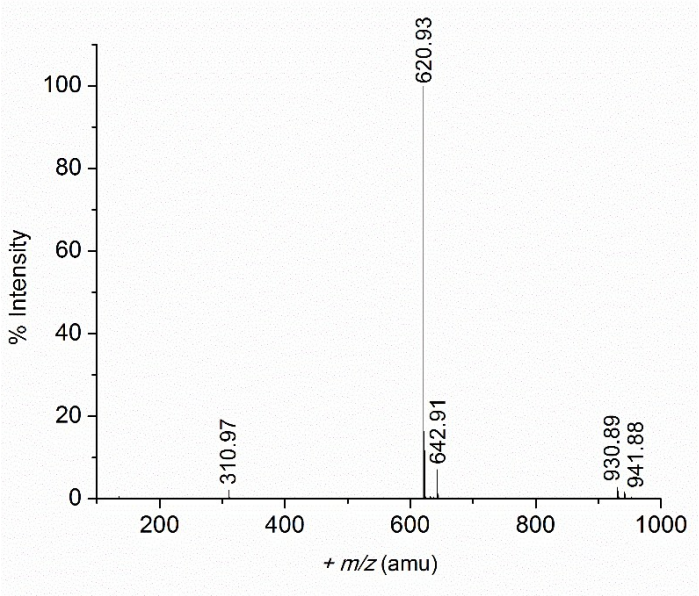

m/z	Assignment
310.97	$[2Rh^{II} + 2AcO^{-} + 2HMet]^{2+}$
620.93	$[2Rh^{II} + 2AcO^{-} + 2HMet - H^{+}]^{+}$
642.91	$[2Rh^{II} + 2AcO^{-} + 2HMet - 2H^{+} + Na^{+}]^{+}$
930.89	$[6Rh^{II} + 6AcO^{-} + 6HMet - 4H^{+}]^{2+}$
941.88	$[6Rh^{II} + 6AcO^{-} + 6HMet - 5H^{+} + Na^{+}]^{2+}$

Figure S5. *Left*) (+)-Ion mode ESI-mass spectra of $[Rh_2(AcO)_2(Met)_2]\cdot 5H2O$ (**2**) and *right*) assignment of the corresponding mass peaks.

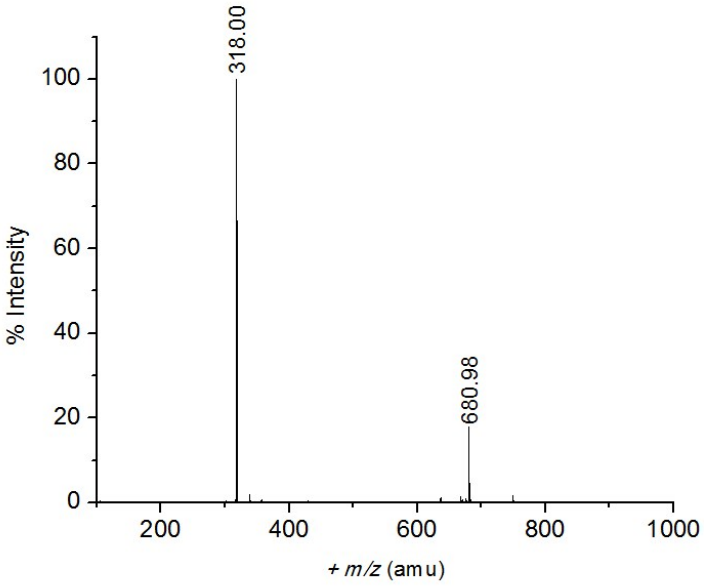

m/z	Assignment
318.00	$[2Rh^{II} + 2AcO^{-} + 2bpy]^{2+}$
680.98	$[2Rh^{II} + 2AcO^{-} + 2bpy + HCOO^{-}]^{+}$

Figure S6. *Left*) (+)-Ion mode ESI-mass spectra of $[Rh_2(AcO)_2(bpy)_2](AcO)_2$ (**3**) and *right*) assignment of the corresponding mass peaks.

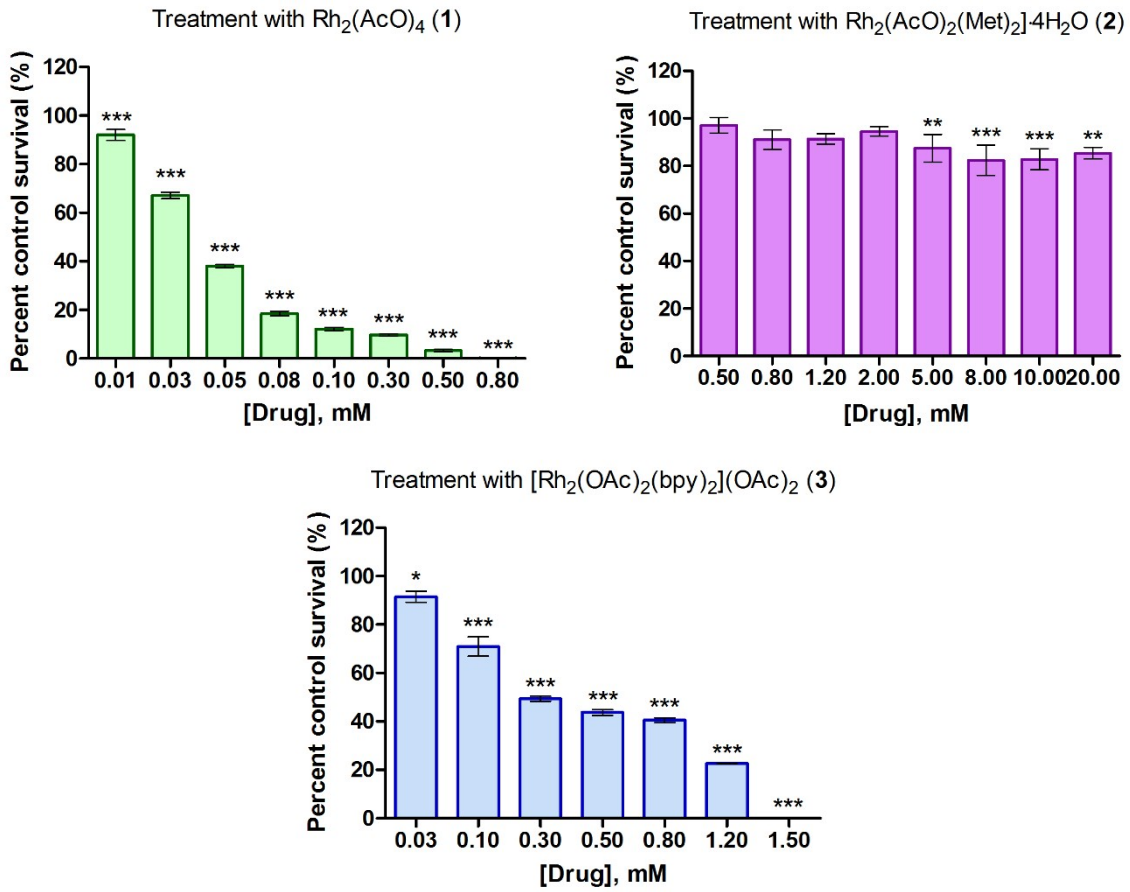

Figure S7. Cell viability plots for MDA-MB-231 cells treated with different increasing concentrations of the three dirhodium(II) complexes: *top left*) $Rh_2(AcO)_4$ (**1**), *top right*) $[Rh_2(AcO)_2(Met)_2]\cdot 5H_2O$ (**2**) and *bottom*) $[Rh_2(AcO)_2(bpy)_2](AcO)_2$ (**3**). Viability of untreated cell cultures was set to 100%. Error bars represent standard deviations. Data were analyzed with a one-way ANOVA followed by Dunnett post-tests: * $p < 0.05$; ** $p < 0.01$; *** $p < 0.001$ from comparisons between treated and control cells.

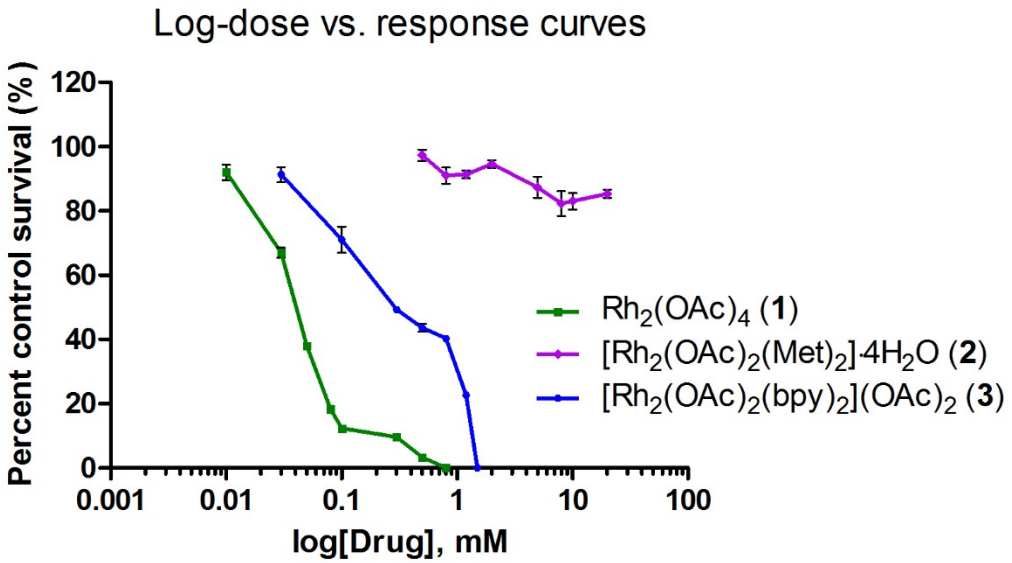

Figure S8. Dose-response curves in MDA-MB-231 cells for all three dirhodium(II) complexes: $Rh_2(AcO)_4$ (**1**), $[Rh_2(AcO)_2(Met)_2]\cdot 5H_2O$ (**2**) and $[Rh_2(AcO)_2(bpy)_2](AcO)_2$ (**3**). Error bars represent standard deviation from the mean and they are not visible if smaller than symbol size.

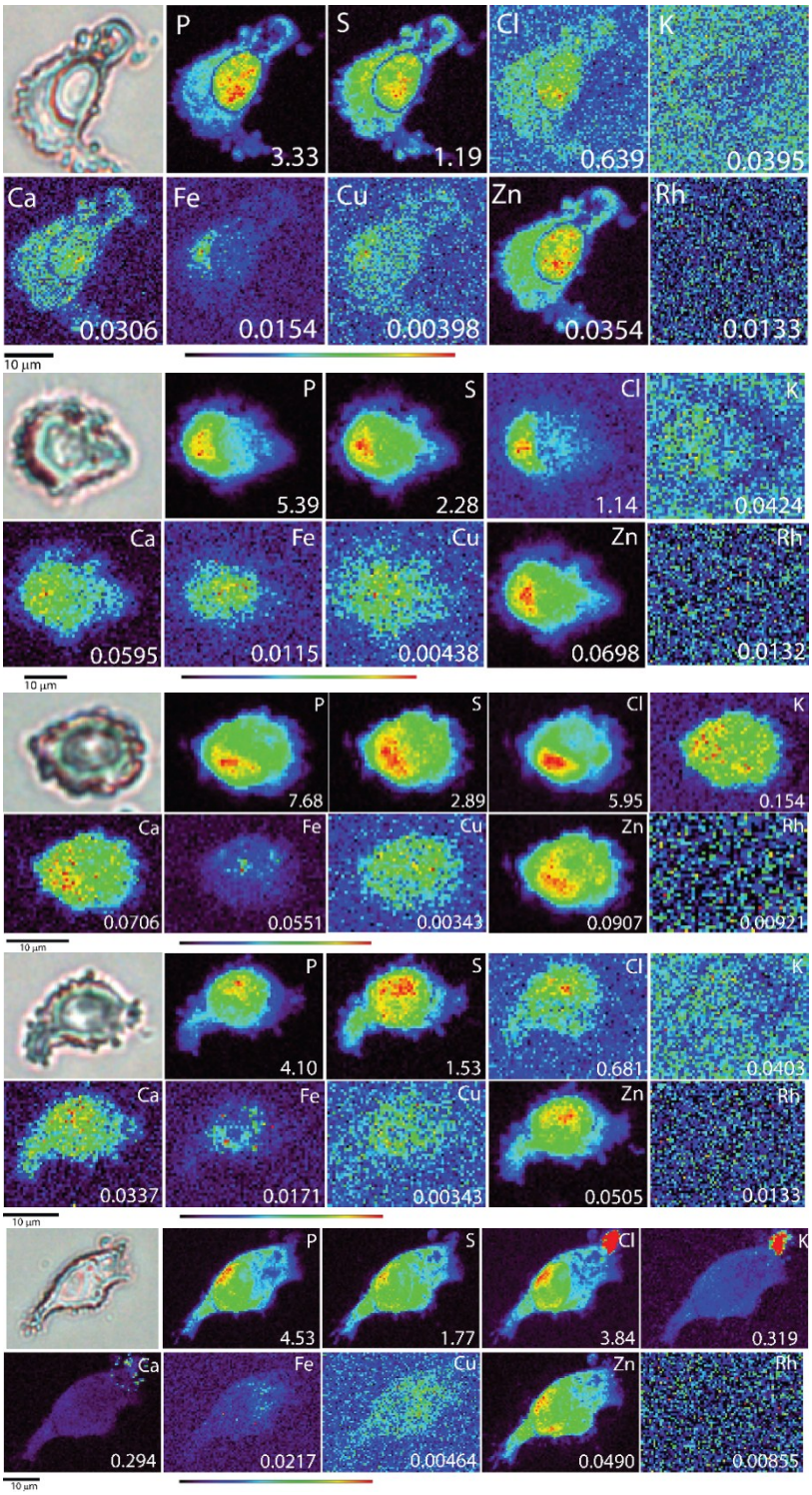

Figure S9. Optical micrographs (top left), and XFM elemental distribution maps of P, S, Cl, K, Ca, Fe, Cu, Zn, and Rh of five MDA-MB-231 cells treated with DMEM media only as control for 6 hr. The maximal elemental area density (in µg/cm^2) is given in the bottom corner of each map. ($E_{incident}$ = 23.8 keV for Rh, Fe, Cu, Zn, and 12.8 keV for low Z elements, i.e. P, S, Cl, K, Ca)

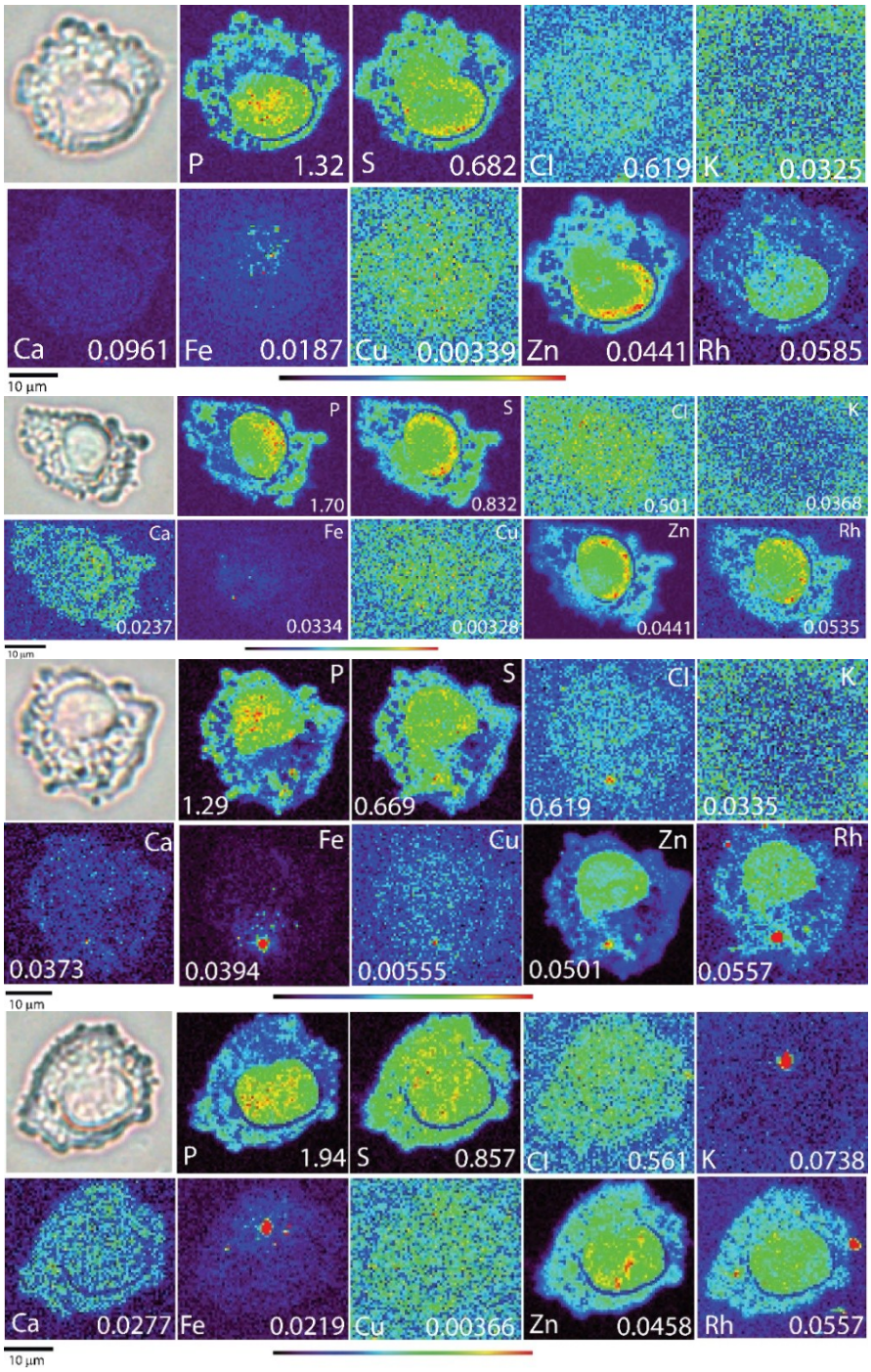

Figure S10. Optical micrographs (top left), and XFM elemental distribution maps of P, S, Cl, K, Ca, Fe, Cu, Zn, and Rh of four MDA-MB-231 cells treated for 6 hr with a 200µM solution $Rh_2(AcO)_4$ (**1**). The maximal elemental area density (in µg/cm^2) is given in the bottom corner of each map. Spots with high concentration of a specific element (artifacts) were removed for quantification. ($E_{incident}$ = 23.8 keV for Rh, Fe, Cu, Zn, and 12.8 keV for low Z elements)

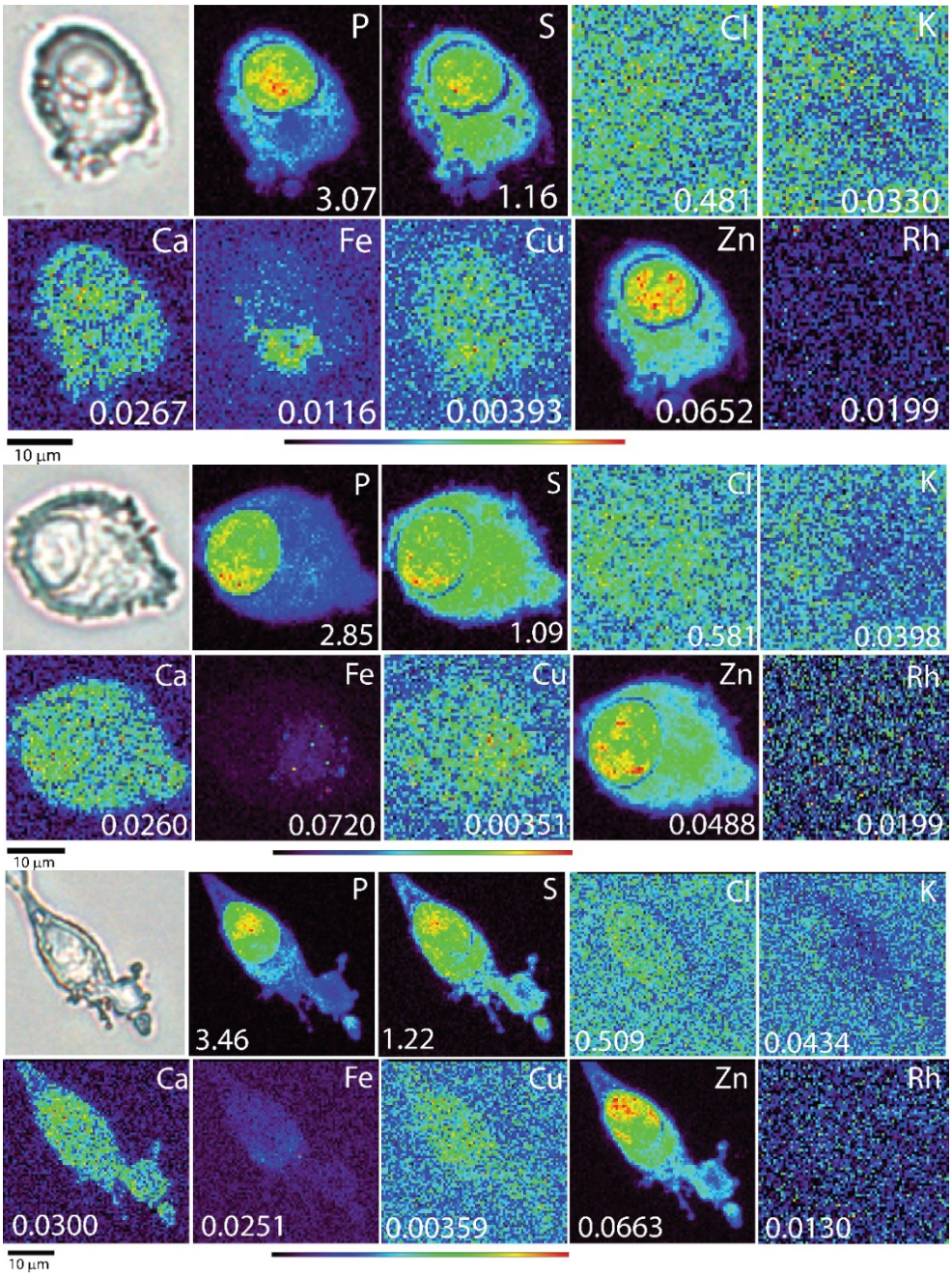

Figure S11. Optical micrographs (top left), and XFM elemental distribution maps of P, S, Cl, K, Ca, Fe, Cu, Zn, and Rh of three MDA-MB-231 cells treated for 6 hr with a 200 µM solution $[Rh_2(AcO)_2(Met)_2]\cdot 5H_2O$ (**2**). The maximal elemental area density (in µg/cm^2) is given in the bottom corner of each map. ($E_{incident}$ = 23.8 keV for Rh, Fe, Cu, Zn, and 12.8 keV for low Z elements)

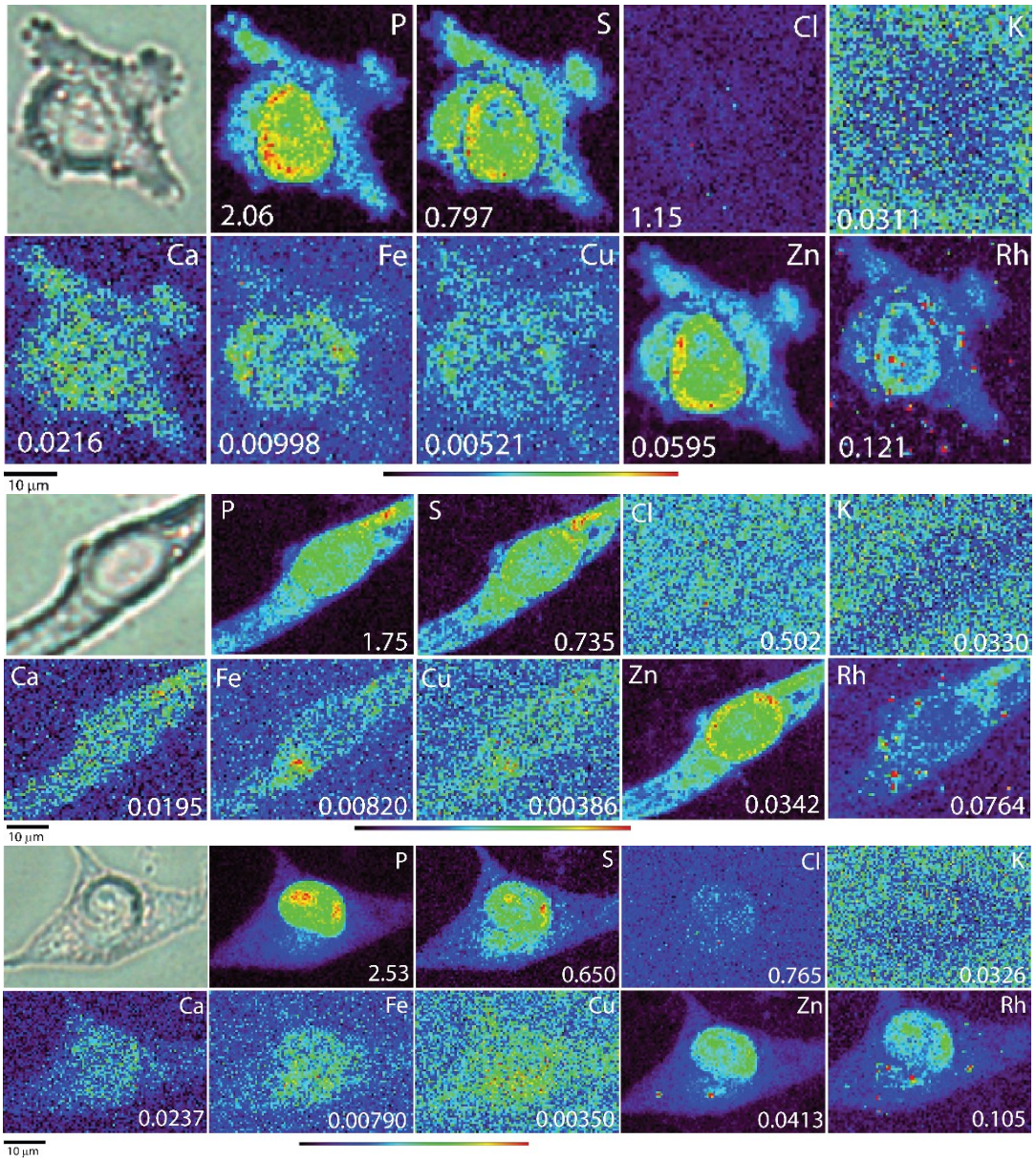

Figure S12. Optical micrographs (top left), and XFM elemental distribution maps of P, S, Cl, K, Ca, Fe, Cu, Zn, and Rh of three MDA-MB-231 cells treated for 6 hr with a 200 µM solution $[Rh_2(OAc)_2(bpy)_2](AcO)_2$ (**3**). The maximal elemental area density (in µg/cm^2) is given in the bottom corner of each map. ($E_{incident}$ = 23.8 keV for Rh, Fe, Cu, Zn, and 12.8 keV for low Z elements)

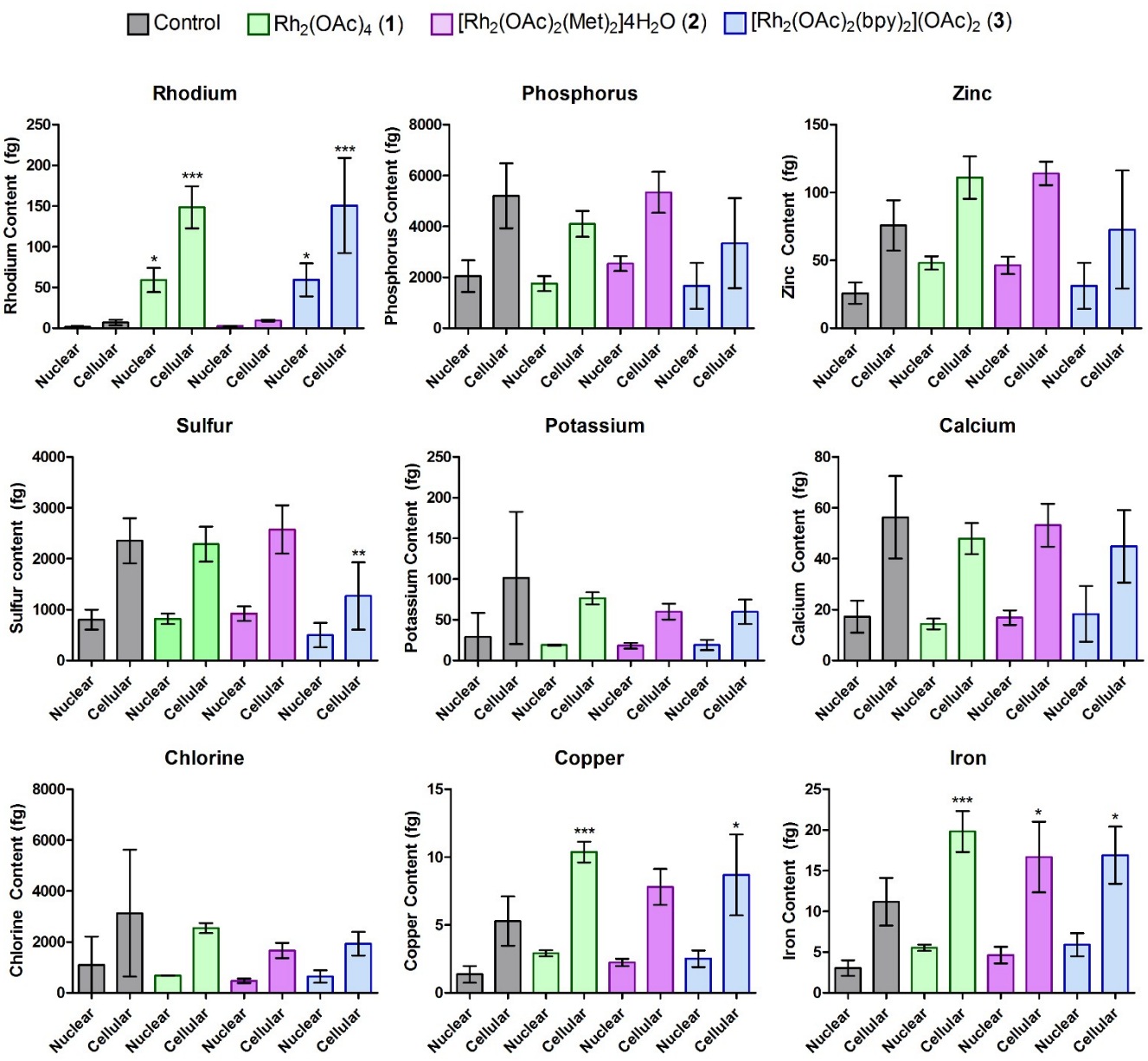

Figure S13. Intracellular content of P, S, Cl, K, Ca, Fe, Cu, Zn, and Rh obtained by quantification using XFM as compared with the nuclear content of MDA-MB-231 cells treated for 6 hr with control (black, n=5) as well as 200 μM solutions of $Rh_2(AcO)_4$ (**1**, green), $[Rh_2(AcO)_2(Met)_2]\cdot 5H_2O$ (**2**, pink) or $[Rh_2(AcO)_2(bpy)_2](AcO)_2$ (**3**, blue) in DMEM. Error bars represent standard deviations. Data were analyzed with a one-way ANOVA followed by Tukey post-tests: *$p < 0.05$; ** $p < 0.01$; *** $p < 0.001$.

Table S1. Quantified total average (n=4) intracellular and nuclear Rh content as well as its nuclear-to-cellular percentage for MDA-MB-231 cells treated for 6 hr with 200 μM solutions of $Rh_2(AcO)_4$ (**1**), $[Rh_2(AcO)_2(Met)_2]\cdot 5H_2O$ (**2**), or $[Rh_2(AcO)_2(bpy)_2](AcO)_2$ (**3**) in DMEM. Values obtained from the quantification of Rh using XFM in different regions of interest: the nucleus and the cell as a whole.

Complex	Cellular Rh content (fg)	Nuclear Rh content (fg)	Nuclear-to-cellular ratio (%)
$Rh_2(AcO)_4$ (**1**)	149 ± 26	59 ± 15	39.6
$[Rh_2(AcO)_2(Met)_2]\cdot 5H_2O$ (**2**)	9 ± 1.1	2.6 ± 0.3	28.9
$[Rh_2(AcO)_2(bpy)_2](AcO)_2$ (**3**)	151 ± 58	59 ± 20	39.1

Table S2. Dipole moments obtained from the DFT calculations performed on the optimized geometries of $Rh_2(AcO)_4$ (**1**), $[Rh_2(AcO)_2(Met)_2]$ (**2**) and $[Rh_2(AcO)_2(bpy)_2]^{2+}$.

Complex	DFT-calculated dipole moment (Debye)[1]
$Rh_2(AcO)_4$ (**1**)	0
$[Rh_2(AcO)_2(Met)_2]$ (**2**)	7.22
$[Rh_2(AcO)_2(bpy)_2]^{2+}$	11.07

[1] These dipole moments were calculated in the gas phase and may not be a true representation of the molecular/ ion polarity in the cell media.

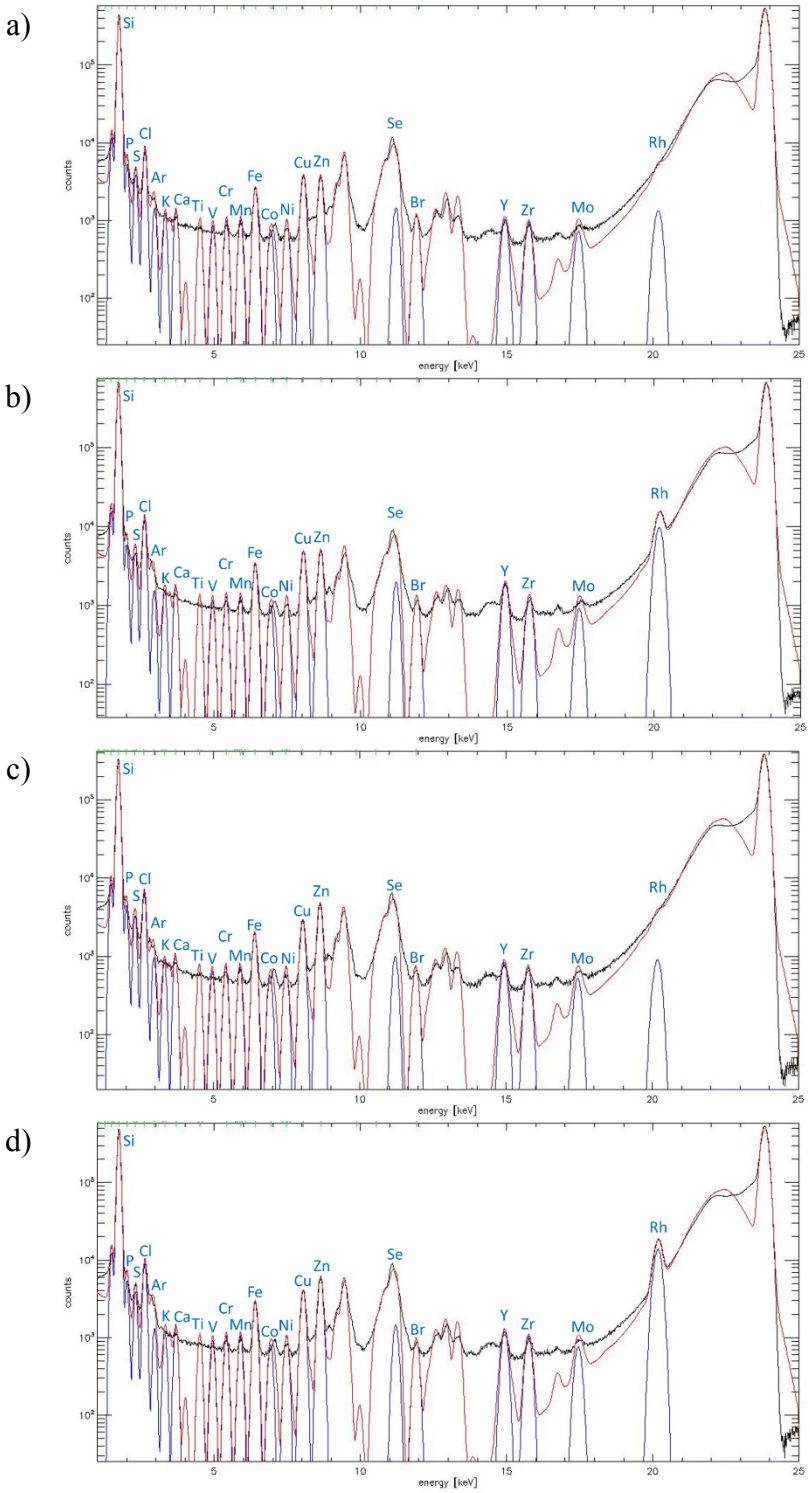

Figure S14. XFM spectra (black) of MDA-MB-231 sample cells treated for 6 hr with: a) only DMEM as control, and 200 μM solutions of b) $Rh_2(AcO)_4$ (**1**), c) $[Rh_2(AcO)_2(Met)_2]\cdot 5H_2O$ (**2**), or d) $[Rh_2(AcO)_2(bpy)_2](AcO)_2$ (**3**) in DMEM. Each figure shows the fit to the spectrum (red), and the contribution of the Kα peaks used in the fitting (blue) with their corresponding labelling.

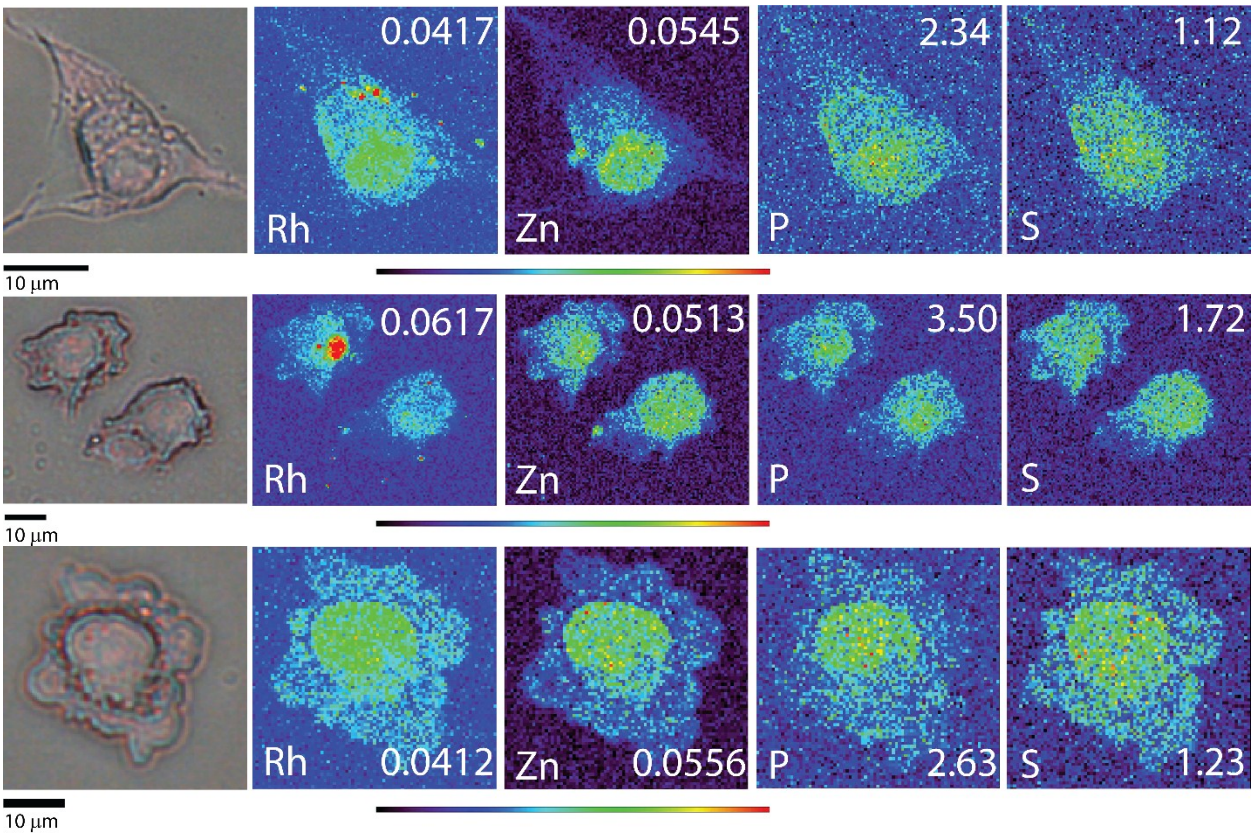

Figure S15. Optical micrographs (left), and XFM elemental distribution maps of P, S, Zn, and Rh of four MDA-MB-231 cells treated for 1 hr with a 200μM solution $Rh_2(AcO)_4$ (**1**). The maximal elemental area density (in μg/cm^2) is given in the top right or bottom right corner of each map. ($E_{incident}$ = 23.8 keV)

References

1. A. Enriquez Garcia, F. Jalilehvand, P. Niksirat and B. S. Gelfand, *Inorg. Chem.*, 2018, **57**, 12787-12799.
2. C. A. Crawford, J. H. Matonic, J. C. Huffman, K. Folting, K. R. Dunbar and G. Christou, *Inorg. Chem.*, 1997, **36**, 2361-2371.
3. M. J. O'Neil, P. E. Heckelman, C. B. Koch and K. J. Roman, eds., *The Merck Index: An Encyclopedia of Chemicals, Drugs, and Biologicals, 14th ed.* , Merck Co., Inc., Whitehouse Station, NJ, 2006.
4. T. D. W. Claridge, in *High-Resolution NMR Techniques in Organic Chemistry (Third Edition)*, ed. T. D. W. Claridge, Elsevier, Boston, 2016, ch. 3, pp. 61-132.
5. *IC50 determination was performed using GraphPad Prism version 5.03 for Windows, GraphPad Software,* www.graphpad.com, La Jolla, California, USA.
6. M. M. Gottesman, T. Fojo and S. E. Bates, *Nat. Rev. Cancer*, 2002, **2**, 48.
7. G. Szakács, J. K. Paterson, J. A. Ludwig, C. Booth-Genthe and M. M. Gottesman, *Nat. Rev. Drug Discov.*, 2006, **5**, 219.
8. J. I. Fletcher, M. Haber, M. J. Henderson and M. D. Norris, *Nat. Rev. Cancer*, 2010, **10**, 147.
9. N. Walsh, S. Kennedy, A. M. Larkin, D. Tryfonopoulos, A. J. Eustace, T. Mahgoub, C. Conway, I. Oglesby, D. Collins, J. Ballot, W. S. Ooi, G. Gullo, M. Clynes, J. Crown and L. O'Driscoll, *Br. J. Cancer*, 2010, **102**, 1157.
10. M. Saxena, M. A. Stephens, H. Pathak and A. Rangarajan, *Cell Death & Disease*, 2011, **2**, e179.
11. G. Szakács, J.-P. Annereau, S. Lababidi, U. Shankavaram, A. Arciello, K. J. Bussey, W. Reinhold, Y. Guo, G. D. Kruh, M. Reimers, J. N. Weinstein and M. M. Gottesman, *Cancer Cell*, 2004, **6**, 129-137.
12. S. Vogt, *J. Phys. IV*, 2003, 635 - 638.
13. M. J. Frisch, G. W. Trucks, H. B. Schlegel, G. E. Scuseria, M. A. Robb, J. R. Cheeseman, G. Scalmani, V. Barone, G. A. Petersson, H. Nakatsuji, X. Li, M. Caricato, A. V. Marenich, J. Bloino, B. G. Janesko, R. Gomperts, B. Mennucci, H. P. Hratchian, J. V. Ortiz, A. F. Izmaylov, J. L. Sonnenberg, Williams, F. Ding, F. Lipparini, F. Egidi, J. Goings, B. Peng, A. Petrone, T. Henderson, D. Ranasinghe, V. G. Zakrzewski, J. Gao, N. Rega, G. Zheng, W. Liang, M. Hada, M. Ehara, K. Toyota, R. Fukuda, J. Hasegawa, M. Ishida, T. Nakajima, Y. Honda, O. Kitao, H. Nakai, T. Vreven, K. Throssell, J. A. Montgomery Jr., J. E. Peralta, F. Ogliaro, M. J. Bearpark, J. J. Heyd, E. N. Brothers, K. N. Kudin, V. N. Staroverov, T. A. Keith, R. Kobayashi, J. Normand, K. Raghavachari, A. P. Rendell, J. C. Burant, S. S. Iyengar, J. Tomasi, M. Cossi, J. M. Millam, M. Klene, C. Adamo, R. Cammi, J. W. Ochterski, R. L. Martin, K. Morokuma, O. Farkas, J. B. Foresman and D. J. Fox, *Gaussian 16, Revision B.01,* Gaussian, Inc., Walligford, CT (2016).
14. F. A. Cotton, B. G. DeBoer, M. D. LaPrade, J. R. Pipal and D. A. Ucko, *Acta Crystallogr., Sect. B: Struct. Sci*, 1971, **27**, 1664-1671.
15. C. J. Fahrni, *Curr. Opin. Chem. Biol.*, 2007, **11**, 121-127.